Journal of Power Sources 205 (2012) 510–515

Contents lists available at SciVerse ScienceDirect

Journal of Power Sources

journal homepage: www.elsevier.com/locate/jpowsour

Electrochemical capacitors of miniature size with patterned carbon nanotubes and cobalt hydroxide

Chun-Hung Chen [a], Dah-Shyang Tsai [a,*], Wen-Hung Chung [a], Kuei-Yi Lee [b], Yi-Min Chen [b], Ying-Sheng Huang [b]

[a] Department of Chemical Engineering, National Taiwan University of Science and Technology, Taipei 10607, Taiwan
[b] Department of Electronic Engineering, National Taiwan University of Science and Technology, Taipei 10607, Taiwan

ARTICLE INFO

Article history:
Received 16 November 2011
Received in revised form 2 January 2012
Accepted 11 January 2012
Available online 18 January 2012

Keywords:
Miniature electrochemical capacitor
Carbon nanotubes
Vertical alignment
Cobalt hydroxide

ABSTRACT

Two miniature electrochemical capacitors, of high power and sufficient energy capacity, are prepared using photolithography and transferred to a plastic substrate. The preparation procedure involves, inverting a 60 μm thick interdigital pattern of multi-walled carbon nanotubes (CNT) with a Scotch tape, such that the pre-sputtered gold layer at the bottom effectively collects interfacial charge. The equivalent series resistance (ESR) of the symmetric CNT capacitor measures 0.40 Ω cm^2, while that of the asymmetric capacitor with a positive α-Co(OH)$_2$/CNT electrode measures 0.45 Ω cm^2, much less than the as-grown CNT capacitor. Electrodeposited α-Co(OH)$_2$ enhances the cell capacitance significantly, especially in a wide potential window. When operated at current density 20 A g^{-1} and window 1.8 V, the cell capacitance of asymmetric capacitor measures 62.6 F g^{-1}, much higher than that of symmetric capacitor 8.7 F g^{-1}. But the symmetric CNT capacitor displays a better power performance because of a lower ESR. At current density 30 A g^{-1}, its power density reaches 20.6 kW kg^{-1} with energy density 2.2 Wh kg^{-1}. In contrast, the asymmetric capacitor stores more energy, at 30 A g^{-1}, it exhibits power density 11.4 kW kg^{-1} and energy density 7.8 Wh kg^{-1}.

1. Introduction

Electrochemical capacitors, also known as ultracapacitors or supercapacitors, are auxiliary devices for the primary energy sources, such as battery and fuel cell. They are characterized with high power capability and long cycle life, which make them ideal in handling intermittent high energy pulses. To strengthen these two attributes, many researchers have incorporated carbon nanotubes (CNT) in the electrode compositions to exploit the continuous electrical conductivity of this carbon allotrope [1–5]. Since the production cost of CNT is relatively high, compared with that of the activated carbon made from coconut shells, CNT is generally viewed as an additive, instead of a major component for regular ultracapacitors [6]. Recently, the miniature ultracapacitor of micrometer thick electrodes has been proposed to store photon energy [7] or power the microelectromechanical devices [8–10]. The ultracapacitor of this size employs only a tiny amount of active materials, in contrast to the material quantity of regular ultracapacitors measuring over several centimeters. For a miniature capacitor, the benefits of CNT conductivity and durability counterbalance its additional material cost.

Preparation methods of these small CNT ultracapacitors in literature may be classified into two approaches. One approach implements the as-grown CNT array, which could be a blanket of vertically aligned nanotubes [11], or a designed pattern such as nanotube bundles [12,13]. This approach relies on the technology toolbox of one-dimensional material to shape the electrode morphology. The second approach uses CNT indirectly, involving more processing labor. The grown nanotubes are harvested from the substrate, and re-dispersed in liquids. These suspended nanotubes are then re-assembled on current collectors to mold the porous electrodes via the pulp and paper making [14], the colloidal deposition [15], or electrophoretical deposition [16]. The CNT-based electrodes are sandwiched with an intervening separator to pack into a parallel-plate configuration. Synthesis procedure of the first approach appears more direct and compatible with the thin film technology of integrated circuit. On the other hand, the second approach treats CNT like a raw material for the capacitor, seemingly provides more accessible interface for charge and discharge. The reported power densities of the second approach are high, ~20–100 kW kg^{-1} with impressive values of energy density [14,16].

We have prepared our miniature capacitors using the first approach, which includes patterning the seed layer of aluminum–iron with photolithography and growing vertically

* Corresponding author at: Department of Chemical Engineering, National Taiwan University of Science and Technology, 43 Keelung Road, Section 4, Taipei 10607, Taiwan. Tel.: +886 2 27376618; fax: +886 2 27376644.
E-mail address: dstsai@mail.ntust.edu.tw (D.-S. Tsai).

0378-7753/$ – see front matter © 2012 Elsevier B.V. All rights reserved.
doi:10.1016/j.jpowsour.2012.01.072

aligned and densely populated CNT electrodes. Employment of aluminum buffer enables a vertical CNT wall, critical in keeping the two opposing electrodes electrically isolated during operation. But the aluminum buffer also leads to high contact resistance, which degrades the capacitor power performance [3,12]. In this work, we avoid the resistance problem through sputtering gold on top of the CNT electrodes; invert and transfer the patterned electrodes to a polymeric substrate with a Scotch tape. These additional processing steps preserve the definition of patterned electrode, and enhance the capacitor power considerably. In view of its high power performance and straightforwardness of pattern transfer, this CNT-based capacitor may find applications in mini power supply such as flash drivers of digital camera.

2. Experimental

2.1. Ultracapacitor preparation

We employed the lift-off technique of photolithography to develop an interdigital pattern of seeding layer on a glass substrate (Eagle 2000, Corning). The seeding layer included a 5 nm buffer film of aluminum and 3 nm iron catalyst, sequentially deposited with an electron beam evaporator (PEVA-500E Advanced System Technology). A well-defined CNT pattern of ~60 μm in height was then grown in a tubular reactor at 750 °C with flowing acetylene. Details on photolithography steps and chemical vapor deposition (CVD) can be found elsewhere [12]. The surface of as-grown CNT pattern was then sputtered with gold, using a radio frequency magnetron sputter. The penetration depth of sputtered gold was ~1.0 μm. Next, we applied a double-sided Scotch tape on the sputtered CNT to remove and invert the pattern onto a plastic substrate. The transferred pattern was examined under an optical microscope to assure its integrity.

For electrical wiring of the inverted electrode, a conducting silver paste was applied to glue a copper wire on its 0.3 cm × 0.3 cm lead area, and the bonding was reinforced with the ARON inorganic adhesive and a waterproof organic adhesive. A symmetric capacitor was made, consisting of two opposing comb-like CNT electrodes of equal mass, immersed in the deaerated 1.0 M KOH electrolyte.

2.2. Capacitor notation

The symmetric capacitor was denoted as CNT_CNT. Nominal area of one CNT electrode was 0.024 cm^2, with mass density 3.0×10^{-4} g cm^{-2}, so that the total CNT mass was 1.4×10^{-5} g. CNT mass of the interdigital electrode was too small to be measured directly. The CNT mass density was evaluated, using a CNT blanket film up to several cm^2 in area, grown near the sample in the same CVD batch. This mass value may be slightly overestimated for the inverted and transferred pattern, because of CNT loss in transferring.

The asymmetric capacitor, denoted as CNT_α-$Co(OH)_2$, was prepared with one CNT electrode deposited with cobalt hydroxide and the other without. Potentiostatic deposition of $Co(OH)_2$ was performed in the acidic solution of 0.1 M $Co(NO_3)_2$, with a potential difference −1.0 V between the working electrode and an Ag/AgCl reference. The deposited electrode was washed and dried at 40 °C overnight. Deposited mass of $Co(OH)_2$ was estimated 2.3×10^{-4} g cm^{-2}, using the Faraday's law. With the added mass of $Co(OH)_2$, the mass density of $Co(OH)_2$/CNT electrode became 5.3×10^{-4} g cm^{-2}. The total active mass of CNT_α-$Co(OH)_2$ asymmetric cell was evaluated 2.0×10^{-5} g.

2.3. Material characterization and electrochemical measurements

The phase of cobalt hydroxide was analyzed with an X-ray diffractometer (D2 Phaser, Bruker) equipped with a Cu Kα radiation source (wavelength 0.15406 nm). Morphology of CNT and electrodeposited $Co(OH)_2$ was examined with a field-emission scanning electron microscope (SEM, JSM-6500F, JEOL). Fine structural details were analyzed using a transmission electron microscope (TEM, Tecnai G2 F20, FEI) with a double tilt specimen holder.

Electrochemical characterization of the comb-like single electrode was performed with cyclic voltammetry (CV) in a typical three-electrode setup. While the charge–discharge and the impedance measurements of two capacitors were done in a two-electrode setup. All measurements were carried out at 27 °C in 1.0 M KOH. Voltammograms of the CNT or $Co(OH)_2$/CNT electrode were recorded at various scan rates, with a Ag/AgCl/satKCl electrode (XR820, Radiometer) as reference, a 2 cm^2 platinum plate as counter electrode, and the comb-like electrode as working electrode. Galvanostatic charge–discharge experiments of the miniature cells were controlled using a multichannel potentiostat (1470E Solartron). For the CNT_α-$Co(OH)_2$ asymmetric cell, the CNT electrode was designated as the negative electrode, the $Co(OH)_2$/CNT electrode was the positive electrode. The potential window can be expanded up to 1.8 V, taking advantage of the overpotentials on positive and negative electrodes. Impedance spectra of the two cells were measured with a frequency analyzer (1260 Solartron). Data were recorded over a frequency range of 0.1 Hz–1.0 MHz at open circuit voltage with potential amplitude of 50 mV.

3. Results and discussion

3.1. Electrode structures

Fig. 1 presents the SEM images of patterned electrodes and their morphological details. The interdigital pattern has two electrodes of ten fingers with a finger spacing of 20 μm. Each finger is ~60 μm in height, 200 μm in width, and 2400 μm in length. Fig. 1(a) compares the images of as-grown (inset) and inverted CNT patterns, showing little dimensional changes after inversion and transfer. The inverted CNT surface does appear slightly squashed around the finger edge, in contrast with the even surface of as-grown CNT,

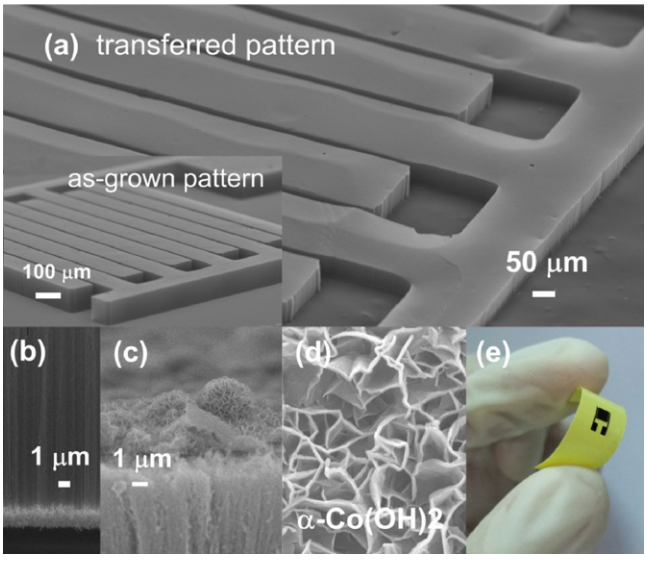

Fig. 1. Images of the interdigital electrodes and microstructures, showing (a) the as-grown CNT electrodes (inset) and the inverted and transferred electrodes; (b) the bottom of inverted nanotubes connected by sputtered gold; (c) the positive electrode decorated with clusters of cobalt hydroxide nanoflakes; (d) the magnified cluster interior being an assembly of α-$Co(OH)_2$ platelets; and (e) the pliable electrodes of CNT_α-$Co(OH)_2$ on a polymer substrate.

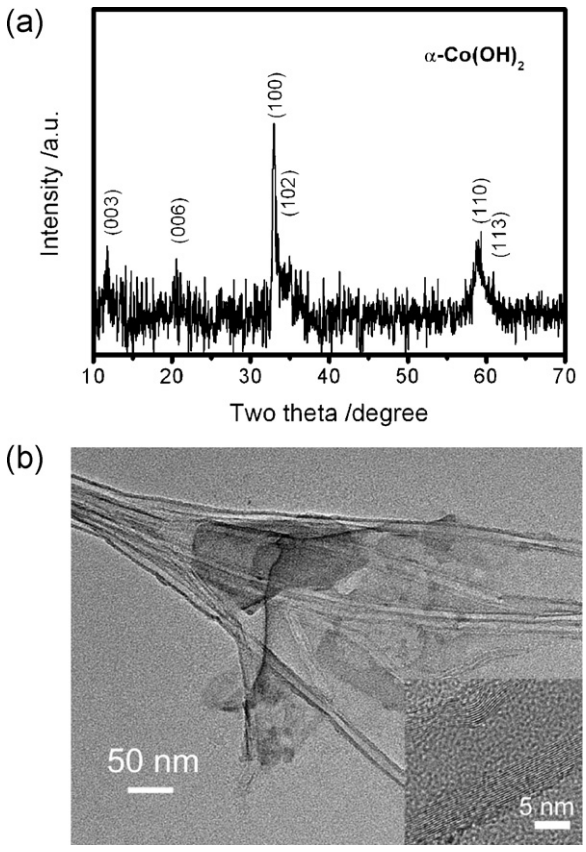

Fig. 2. (a) X-ray diffraction pattern of α phase cobalt hydroxide; (b) a bright field TEM image showing the hydroxide is spanned between CNT. The reflections of (a) are assigned according to JCPDS file no. 46-0605. A high-resolution inset of (b) depicts the lattice fringes of a multi- walled nanotube.

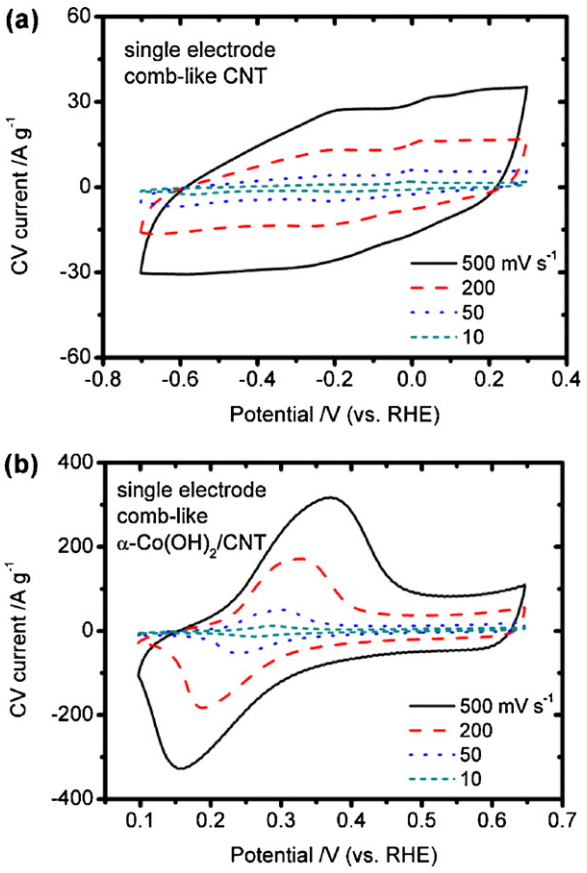

Fig. 3. Cyclic voltammograms of two comb-like electrodes at various scan rates in 1.0 M KOH; (a) CNT electrode, (b) α-$Co(OH)_2$/CNT electrode. The mass-specific current is based on the CNT mass or the mass of α-$Co(OH)_2$ plus CNT.

since the nanotubes array has been pressed during pattern transfer. Still, the wall of inverted electrode on Scotch tape stands vertically, defining the finger boundary precisely. Fig. 1(b) shows the bottom of inverted pattern has been infiltrated by ~1.5 μm sputtered gold, which does not enter farther because nanotubes are densely populated. This sputtered gold serves as the current collector for the inverted CNT electrode. Fig. 1(e) demonstrates the flexibility of the inverted pattern, which is bent on a polymer substrate. The positive electrode of CNT_α-$Co(OH)_2$ capacitor is decorated with a number of micron-sized globules on its exterior, as shown in Fig. 1(c). Each globule consists of many cobalt hydroxide nanoflakes. A magnified SEM image, shown in Fig. 1(d), indicates these nanoflakes are ~10 nm thick and ~300–400 nm wide. This flaky, loosely packed structure has been observed and reported in several papers on the pseudocapacitive α-$Co(OH)_2$ [17–22].

In addition to morphological attributes, we identify the platelet-like crystals to be α-polymorph of $Co(OH)_2$, according to its green-bluish color and X-ray diffraction features. The hydroxide powder sample has been scratched and collected from two electrodeposited $Co(OH)_2$/CNT blanket films, so that we may have a sufficient quantity to analyze. The green-bluish color of α phase distinctively differs from the pink color of β phase. According to Ma et al. [23], this color results from an expanded interlayer spacing of $Co(OH)_2$ basal planes, intercalated with water and anions. X-ray diffraction pattern of the hydroxide powder is plotted in Fig. 2(a). Since the structure of α-$Co(OH)_2$ is still a matter of debate, the reflections in Fig. 2(a) may be assigned in several ways. But it is generally agreed that the two low-angle peaks at $2\theta = 11$ and 22° are 0 0 l reflections which arise from the preferred oriented basal planes [19–23]. They are indexed as (0 0 3) and (0 0 6) reflections, following the JCPDS file 46-0605. The other two reflections at $2\theta = 33$ and 59° are quite broad because of small crystallite size and proximity of neighboring reflections. The broad 33° peak comprises two reflections of (1 0 0) and (1 0 2), while the 59° peak consists of (1 1 0) and (1 1 3) reflections.

Fig. 2(b) depicts a bright-field TEM image, showing the cobalt hydroxide flake is suspended between several carbon nanotubes of 12–18 nm in diameter. These nanotubes are multi-walled, consisting of 15–20 graphene sheets, the lattice fringes are clearly seen in the inset. Although α-$Co(OH)_2$ is a stable phase in an alkaline electrolyte, it is difficult to focus electron beam on the α-$Co(OH)_2$ nanoflake, since the hydroxide is not stable under electron bombardment.

3.2. CV results of comb-like single electrode

Fig. 3 contrasts the voltammograms of CNT and α-$Co(OH)_2$/CNT comb-like electrodes at 10–500 mV s^{-1}. Nearly rectangular voltammograms are recorded between −0.7 and 0.3 V (vs. RHE) for the CNT comb-like electrode, as shown in Fig. 3(a), suggesting its capacitance dominated by double-layer capacitance. Values of CV capacitance are calculated, using the equation $Q_{CV}/2(m_{CNT} \times \Delta V)$, where Q_{CV} is the sum of anodic and cathodic charge, m_{CNT} is the CNT electrode mass, ΔV is the potential range. Table 1 lists that CV capacitance value of single CNT electrode, which progressively decreases with increasing scan rate.

On the other hand, the voltammograms of α-$Co(OH)_2$/CNT electrode display a pair of strong redox peaks between 0.10 and 0.65 V, as illustrated in Fig. 3(b). The evident current peaks indicate the measured capacitance is dominated by pseudocapacitance, which

Table 1
Values of CV capacitance for the comb-like CNT and α-$Co(OH)_2$/CNT electrodes. The potential window of CV measurements is between −0.7 and 0.3 V for CNT electrode, between 0.1 and 0.65 V (vs. RHE) for α-$Co(OH)_2$/CNT electrode.

Scan rate ($mV\,s^{-1}$)	CNT ($F\,g^{-1}$)	α-$Co(OH)_2$/CNT ($F\,g^{-1}$)
5	109	505
10	107	392
50	73	303
200	54	279
500	44	244

most probably arises from the redox reactions between Co(II) and Co(III) [19–21]. The CV capacitance value of α-$Co(OH)_2$/CNT is high, but decreases very rapidly from 5 to 50 $mV\,s^{-1}$. The decreasing trend slows down when the scan rate is higher than 50 $mV\,s^{-1}$, as shown in Table 1. The highest capacitance value of α-$Co(OH)_2$/CNT electrode is 505 $F\,g^{-1}$, considerably less than the values reported in literature for α-$Co(OH)_2$, 860 $F\,g^{-1}$ [19] and 1473 $F\,g^{-1}$ [21]. Our α-$Co(OH)_2$/CNT capacitance is less, because our electrode contains CNT and α-$Co(OH)_2$ both and the specific capacitance of CNT is lower than that of α-$Co(OH)_2$.

3.3. Impedance spectra

Fig. 4 compares the impedance spectra of CNT_CNT and CNT_α-$Co(OH)_2$ cells. The two Nyquist plots intersect the real axis at an angle of ~45°, which is characteristic of ion diffusion in a porous electrode. Intercepts of the two impedance curves are practically the same, ~5 Ω, denoting the equal electrolyte resistance for the two cells because of the identical finger spacing 20 μm. Although the electrolyte resistance is the same, their electrode resistances are different. Addition of α-phase cobalt hydroxide increases the electrode resistance, since cobalt hydroxide is less conductive than CNT. The higher electrode resistance of α-$Co(OH)_2$/CNT is manifested in the equivalent series resistance (ESR) value of its capacitor, defined as the real part of impedance at 1 kHz to symbolize the cell resistance. As marked in Fig. 4, the ESR value of the symmetric CNT_CNT capacitor is 8.3 Ω (0.40 Ω cm^2), while that of the asymmetric CNT_α-$Co(OH)_2$ capacitor is 9.3 Ω (0.45 Ω cm^2). The cell resistance of CNT_α-$Co(OH)_2$ is higher by 1.0 Ω, which is attributed to the extra resistance of cobalt hydroxide. The two ESR values are much less than that of the symmetric cell made of as-grown CNT without sputtered gold, 47.0 Ω cm^2.

The inset of Fig. 4 shows the Bode plots for the impedance of CNT_CNT and CNT_α-$Co(OH)_2$. In the low frequency region, the tilted line of CNT_CNT lies above that of CNT_α-$Co(OH)_2$, because

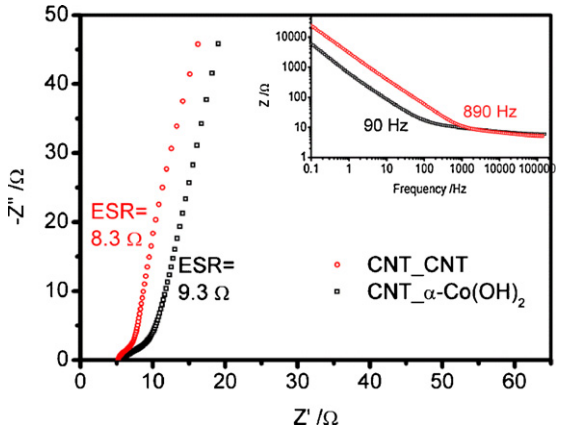

Fig. 4. Impedance spectra of the symmetric CNT_CNT cell and the asymmetric CNT_α-$Co(OH)_2$ cell. The inset shows Bode plots of these two cells, with the knee frequency marked for each cell.

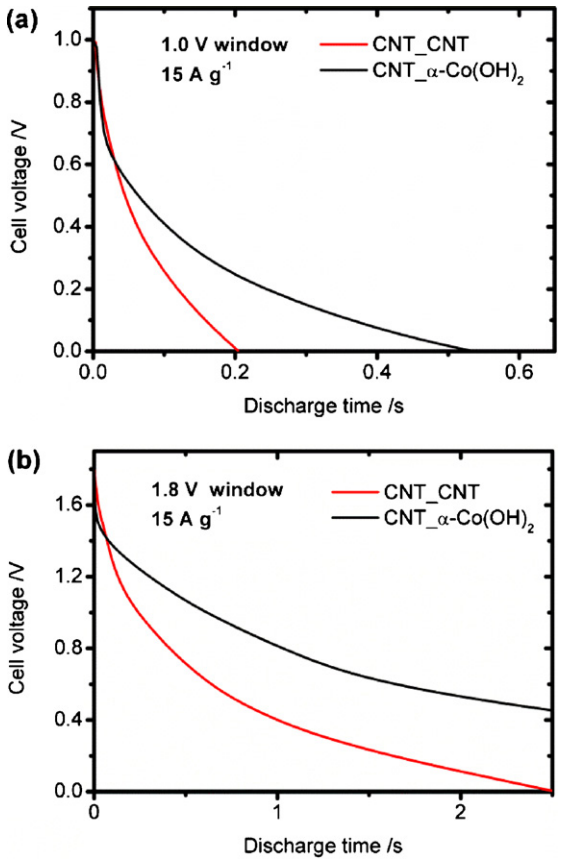

Fig. 5. Galvanostatic discharge curves of the CNT_CNT and CNT_α-$Co(OH)_2$ cells at the current density 15 $A\,g^{-1}$ in the potential window of (a) 1.0 V and (b) 1.8 V.

the imaginary part of CNT_CNT is significantly larger. The large $|Z''|$ value means a small capacitance, and suggests CNT_CNT being a more rapid response capacitor than CNT_α-$Co(OH)_2$. We define the knee frequency as the frequency at which the horizontal line of high frequency region changes into the tilted line of low frequency region. Although the knee frequency is not a precisely defined value, its order of magnitude still provides a legitimate indication. For CNT_CNT, the knee frequency is estimated to be 890 Hz, significantly higher than 90 Hz of CNT_α-$Co(OH)_2$. The two knee frequencies are much higher than that of most commercially available supercapacitors which is generally less than 1 Hz, but less than the very high knee frequency 7560 Hz that is reported on the parallel-plate capacitor of electrophoretically deposited multi-walled CNT [3].

3.4. Galvanostatic charge discharge results

Fig. 5(a) compares the cell voltage variations with time at current density 15 $A\,g^{-1}$ during energy discharge of CNT_CNT and CNT_α-$Co(OH)_2$. In the potential window of 1.0 V, since the CNT_CNT cell has a small capacity and a small ohmic resistance, it discharges its energy in 0.20 s with little IR drop. Alternatively, the CNT_α-$Co(OH)_2$ cell has a larger capacity and the discharge time is longer, 0.53 s. The voltage of this asymmetric capacitor also descends more rapidly at the beginning. The potential curves of two cells intersect at 0.61 V. Between 1.0 and 0.61 V, the potential of CNT_α-$Co(OH)_2$ descends faster than CNT_CNT. When the potential is lower than 0.61 V, the cell voltage of CNT_CNT descends more rapidly.

Taking advantage of electrode overpotentials, the charge and discharge experiments of CNT_CNT and CNT_α-$Co(OH)_2$ can be

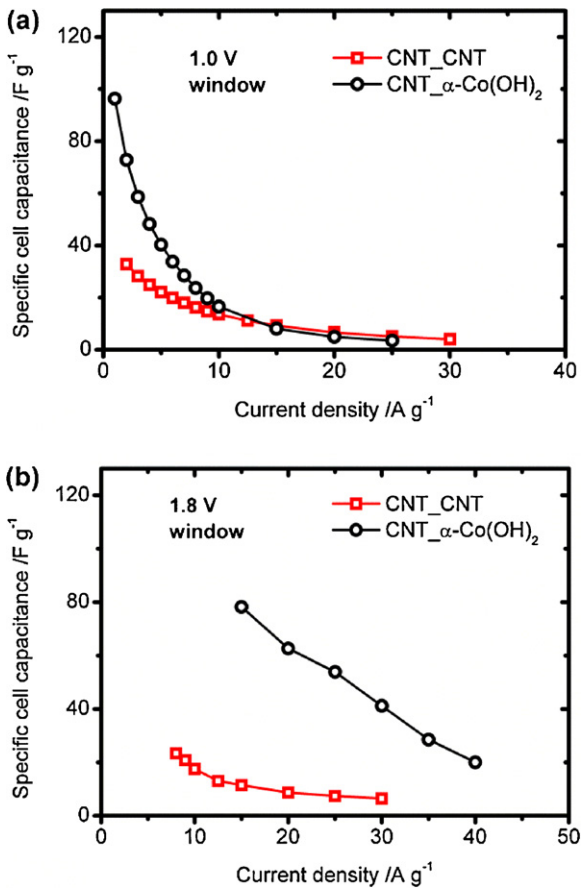

Fig. 6. Variations of the cell capacitance versus current density for CNT_CNT and CNT_α-$Co(OH)_2$ in the potential window of (a) 1.0 V and (b) 1.8 V. The specific cell capacitance is calculated, based on the discharge curve of capacitor.

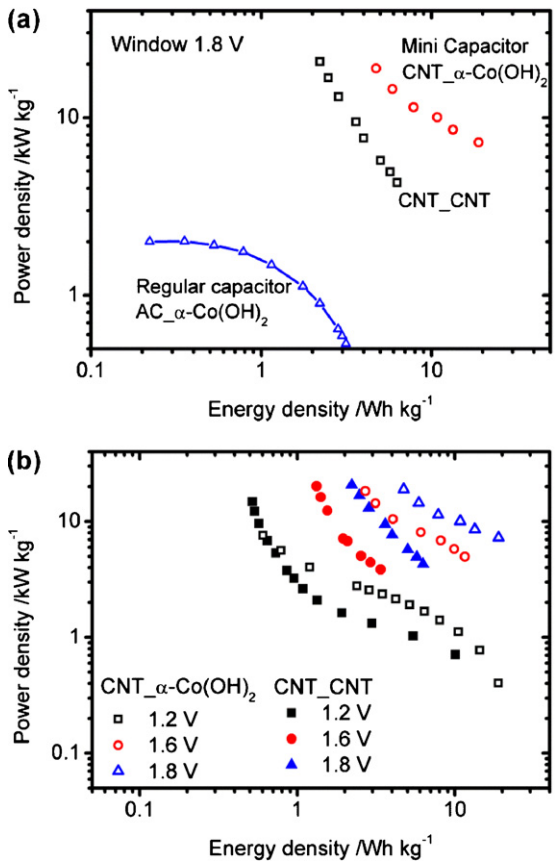

Fig. 7. (a) Ragone plots of CNT_CNT and CNT_α-$Co(OH)_2$ miniature capacitors and the Ragone plot of AC_α-$Co(OH)_2$ reference capacitor. (b) Ragone plots of CNT_CNT and CNT_α-$Co(OH)_2$ in the potential windows of 1.2, 1.6, and 1.8 V.

operated in an expanded potential window of 1.8 V. Fig. 5(b) shows the two cell voltages descend in a similar way, they intersect at 1.42 V. Hence, except a brief early moment, the CNT_α-$Co(OH)_2$ cell discharges at a higher cell potential than the CNT_CNT cell. With the extra energy storage in α-$Co(OH)_2$ pseudocapacitance, the discharge time of CNT_α-$Co(OH)_2$ is much longer. At current density 15 A g^{-1}, the discharge time is 6.41 s for CNT_α-$Co(OH)_2$, and 2.52 s for CNT_CNT.

Fig. 6 presents the specific cell capacitances of CNT_CNT and CNT_α-$Co(OH)_2$ when discharge in two potential windows of 1.0 and 1.8 V. The value of specific cell capacitance is calculated as the integral of discharge current with respect to time divided by the potential window and the active material mass of two electrodes. Fig. 6(a) shows that, in the 1.0 V window, the specific capacitance values of both cells decreases with increasing current density, but the specific capacitance of CNT_α-$Co(OH)_2$ descends more dramatically than that of CNT_CNT. At a current density < 12 A g^{-1}, the specific capacitance of CNT_α-$Co(OH)_2$ is higher than that of CNT_CNT. At a current density > 12 A g^{-1}, the specific capacitance of CNT_α-$Co(OH)_2$ is similar, or slightly less than that of CNT_CNT. Nevertheless, because of the extra α-$Co(OH)_2$ mass of CNT_α-$Co(OH)_2$, the cell capacitance of CNT_α-$Co(OH)_2$ is still higher than that of CNT_CNT up to 25 A g^{-1}. In the high current density region, 20–30 A g^{-1}, the capacitance difference between two cells is small.

When operated in the 1.8 V window, the specific capacitance value of CNT_α-$Co(OH)_2$ is significantly higher than that of CNT_CNT, as shown in Fig. 6(b). Quantitatively, the specific capacitance of CNT_α-$Co(OH)_2$, at current density 30 A g^{-1}, is 41.1 F g^{-1}, while that of CNT_CNT is only 6.4 F g^{-1}. Hence the pseudocapacitance of extra cobalt hydroxide comes into effect, especially in a wide potential window. If the potential widow is narrow, such as 1.0 V, the pseudocapacitance effect of cobalt hydroxide is restricted in the low current density region.

Based on the discharge results, we calculate the values of energy density E and power density P using the following equations;

$$E = i\int_{t_{max}}^{t_0} V_{cell}(t)dt \quad (1)$$

$$P = \frac{E}{\Delta t} \quad (2)$$

in which i is the current density, V_{cell} the cell voltage. The upper and low limits denote the start time (t_{max}) and end time (t_0) when V_{cell} descends from its maximum value to zero, and Δt stands for the time interval between t_{max} and t_0. Fig. 7(a) compares the Ragone plots of two miniature capacitors, CNT_CNT and CNT_α-$Co(OH)_2$, with that of a reference capacitor AC_α-$Co(OH)_2$ in the potential window 1.8 V. The reference AC_α-$Co(OH)_2$ is a regular size capacitor of parallel-plate configuration, with a negative electrode of activated carbon (AC) and a positive electrode of 90 wt.% AC and 10 wt.% α-$Co(OH)_2$. Evidently, the energy density of parallel-plate capacitor decreases rapidly when the power reaches a critical level, ~2 kW kg^{-1}, resulting in the "knee" shaped curve common to most of ultracapacitors. On the other hand, the Ragone plots of miniature CNT_CNT and CNT_α-$Co(OH)_2$ are nearly straight lines, suggesting their reductions in energy exchange for power increase more effectively. Furthermore, when we compare the power density of CNT_CNT with that of AC_α-$Co(OH)_2$ at energy density ~2 Wh kg^{-1}, the power density of miniature capacitor is higher than the regular capacitor by one order of magnitude. The enhanced power

performance of miniature capacitor is attributed to the superior conductivity of CNT, compared with activated carbon.

When the energy and power densities of CNT_CNT and CNT_α-$Co(OH)_2$ are compared, we note that they are similar in power density, different in energy density. Hence their linear Ragone plots have quite different slopes. Fig. 7(a) shows the slope of CNT_CNT is steeper than that of CNT_α-$Co(OH)_2$. A steep slope means the energy density of CNT_CNT does not decline as much as CNT_α-$Co(OH)_2$ for the same amount of power increment. This difference is attributed to the smaller ESR and capacitance of CNT_CNT.

Fig. 7(b) shows that the power and energy densities of CNT_CNT and CNT_α-$Co(OH)_2$ in three potential windows, 1.2, 1.6, and 1.8 V. When the potential window is 1.2 V, the two mini capacitors also display the "knee" shaped curves. When the potential window is 1.6 or 1.8 V, the curves become linear. Owing to the small internal resistance, CNT_CNT is a high-power capacitor, when discharge at 1.8 V and 30 A g^{-1}, this miniature capacitor exhibits power density 20.6 kW kg^{-1} (6.2 mW cm^{-2}) and energy density 2.2 Wh kg^{-1} (2.4 mWs cm^{-2}). The power level of CNT_CNT cell is comparable to that of the electrophoretically deposited CNT film capacitor [3] and that of the single-walled CNT cell with a nickel current collector [24]. The power and energy densities of CNT_CNT cell in 1.8 V is analogous to those of the CNT_α-$Co(OH)_2$ cell in a smaller window 1.6 V. When CNT_α-$Co(OH)_2$ operated in 1.8 V, it exhibits more energy capacity at the similar power level. For instance, at current density of 40 A g^{-1}, the power density of CNT_α-$Co(OH)_2$ is raised to 19.0 kW kg^{-1} (7.9 mW cm^{-2}) with the energy density 4.7 Wh kg^{-1} (7.1 mWs cm^{-2}), which is comparable to the performance of asymmetric CNT capacitors [25]. The energy capacity of CNT_α-$Co(OH)_2$ is generally 3–4 times that of CNT_CNT.

4. Conclusions

To reduce the electrode resistance and sufficiently utilize the surface area of densely populated CNT, we have sputtered the interdigital electrodes with gold, inverted and transferred the patterned electrode onto a polymer substrate such that the sputtered gold layer can effectively collect charge of the porous electrode. Two flexible capacitors are prepared; the symmetric capacitor CNT_CNT and asymmetric capacitor CNT_α-$Co(OH)_2$. Their electrode resistances are significantly reduced, as evidenced in their ESR values; 0.40 Ω cm^2 for CNT_CNT, and 0.45 Ω cm^2 for CNT_α-$Co(OH)_2$, in contrast to 47.0 Ω cm^2 for the as-grown CNT cell. Although α-$Co(OH)_2$ raises the electrode resistance, it also enhances the cell energy capacity. When compared at the same current density 30 A g^{-1}, the energy density of CNT_α-$Co(OH)_2$ 7.8 Wh kg^{-1} is much higher than 2.2 Wh kg^{-1} of CNT_CNT.

Acknowledgements

This work is financially supported by National Science Council of Taiwan through the contract NSC100-2221-E011-079-MY3. We are also grateful to the equipment funding of National Taiwan University of Science and Technology on Nanotechnology Research.

References

[1] H. Pan, J. Li, Y.P. Feng, Nanoscale Res. Lett. 5 (2010) 654–668.
[2] P. Simon, Y. Gogotsi, Nat. Mater. 7 (2008) 845–854.
[3] C. Du, N. Pan, Nanotechnology 17 (2006) 5314–5318.
[4] E. Frackowiak, K. Metenier, V. Bertagna, F. Beguin, Appl. Phys. Lett. 77 (2000) 2421–2423.
[5] C. Niu, E.K. Sichel, R. Hoch, D. Moy, H. Tennent, Appl. Phys. Lett. 70 (1997) 1480–1482.
[6] P.J. Hall, M. Mirzaeian, S.I. Fletcher, F.B. Sillars, A.J.R. Rennie, G.O. Shitta-Bey, G. Wilson, A. Cruden, R. Carter, Energy Environ. Sci. 3 (2010) 1238–1251.
[7] G. Wee, T. Salim, Y.M. Lam, S.G. Mhaisalkar, M. Srinivasan, Energy Environ. Sci. 4 (2011) 413–416.
[8] D. Pech, M. Brune, H. Durou, P. Huang, V. Mochalin, Y. Gogotsi, P.L. Taberna, P. Simon, Nat. Nanotechnol. 5 (2010) 651–654.
[9] J. Chmiola, C. Largeot, P.L. Taberna, P. Simon, Y. Gogotsi, Science 328 (2010) 480–483.
[10] Y.Q. Jiang, Q. Zhou, L. Lin, Proc. of IEEE Int. Conf. on MEMS, Italy, 2009, pp. 587–590.
[11] R. Amade, E. Jover, B. Caglar, T. Mutlu, E. Bertran, J. Power Sources 196 (2011) 5779–5783.
[12] C.C. Liu, D.S. Tsai, W.H. Chung, K.W. Li, K.Y. Lee, Y.S. Huang, J. Power Sources 196 (2011) 5761–5768.
[13] M. Beidaghi, W. Chen, C. Wang, J. Power Sources 196 (2011) 2403–2409.
[14] A. Izadi-Najafabadi, S. Yasuda, K. Kobashi, T. Yamada, D.N. Futaba, H. Hatori, M. Yumura, S. Iijima, K. Hata, Adv. Mater. 22 (2010) E235–E241.
[15] H.R. Byon, S.W. Lee, S. Chen, P.T. Hammond, S.H. Yang, Carbon 49 (2011) 457–467.
[16] C. Du, N. Pan, J. Power Sources 160 (2006) 1487–1494.
[17] L.B. Kong, M. Liu, J.W. Lang, Y.C. Luo, L. Kang, J. Electrochem. Soc. 156 (2009) A1000–A1004.
[18] L.B. Kong, J.W. Lang, M. Liu, Y.C. Luo, L. Kang, J. Power Sources 194 (2009) 1194–1201.
[19] V. Gupta, T. Kusahara, H. Toyama, S. Gupta, N. Miura, Electrochem. Commun. 9 (2007) 2315–2319.
[20] T. Zhao, H. Jiang, J. Ma, J. Power Sources 196 (2011) 860–864.
[21] L.B. Kong, M.C. Liu, J.W. Lang, M. Liu, Y.C. Luo, L. Kang, J. Solid State Electrochem. 15 (2011) 571–577.
[22] R.S. Jayashree, P.V. Kamath, J. Mater. Chem. 9 (1999) 961–963.
[23] R. Ma, Z. Liu, K. Takada, K. Fukuda, Y. Ebina, Y. Bando, T. Sasaki, Inorg. Chem. 45 (2006) 3964–3969.
[24] K.H. An, W.S. Kim, Y.S. Park, J.M. Moon, D.J. Bae, S.C. Lim, Y.S. Lee, Y.H. Lee, Adv. Funct. Mater. 11 (2001) 387–392.
[25] P.C. Chen, G. Shen, Y. Shi, H. Chen, C. Zhou, ACS Nano 4 (2010) 4403–4411.